A Semiautomatic Extraction of Antarctic Lake Features Using Worldview-2 Imagery

Shridhar D. Jawak and Alvarinho J. Luis

Abstract

We devised a semiautomatic approach for extracting lake features based on a customized set of normalized difference water index (NDWI) information which was obtained by incorporating high resolution, 8-band WorldView-2 data. An extensive accuracy assessment was carried out for three semiautomatic feature extraction approaches for extracting 36 lake features on Larsemann Hills, Antarctica. The method was tested on five existing PAN-sharpening algorithms, which suggest that the customized NDWI approach renders intermediate performance (root mean square error varies from ~227 to ~235 m²) and highest stability when compared with existing feature extraction techniques. In general, the customized NDWI rendered a least misclassification (≈11 percent), followed by target detection (≈16 percent) and spectral processing (≈17 percent) methods for extraction of 36 lakes. We also found that customized NDWI caused consistently least misclassification (≈21 percent) than the target detection (≈23 percent) and spectral processing (≈30 percent) methods for extraction of partially snow or ice-covered 11 lakes. Our results indicate that the use of the customized NDWI approach and appropriate PAN-sharpening algorithm can greatly improve the semiautomatic extraction of lake features in cryospheric environment.

Introduction

The semiautomatic (partly automatic or operating with minimal human intervention) feature extraction method interactively attempts to synergistically merge the intelligence or knowledge of human visual system to robustly recognize the targeted feature and the computer-aided system to carry out rapid extraction of targeted feature and accurate shape representation (Hu *et al.*, 2004). In semiautomatic feature extraction strategy, the target feature of interest is first recognized by human vision and some approximations in terms of seed points or training samples about the targeted feature are often provided. The targeted feature is then delineated automatically by the computer-aided algorithm.

Frazier and Page (2000) reviewed numerous methods employed by various authors to extract water bodies from Landsat Thematic Mapper (TM) and Multispectral Scanner (MSS). It is apparent that the most common methods for extracting water bodies use single band-based threshold methods, spectral index ratio (SIR)-based multiband methods, image segmentation methods, spectral-matching methods, and supervised target detection methods.

Presently, the methods for extracting surface water bodies are based on spectral index or multiband techniques, which are spectrum property-based methods, such as the normalized difference vegetation index (NDVI) and the normalized difference water index (NDWI) (McFeeters, 1996; McFeeters, 2013). Because a single spectral index cannot delineate water bodies effectively in different environments, many improved indices have been proposed to obtain better results in a particular environment (Lacaux *et al.*, 2007; Xu, 2005). Ouma and Tateishi (2006) proposed a novel water extraction index for shoreline delineation by combining the tasseled cap wetness index (TCWI) and NDWI. A comprehensive water body information extraction technique was proposed by Wu *et al.* (2008) through fusion of the spectral relationships between various bands with supervised classification methods. Rogers and Kearney (2004) proposed the NDWI for Moderate Resolution Imaging Spectroradiometer (MODIS) multispectral satellite images (MSI). Furthermore, Xiao *et al.* (2005) proposed a land surface water index (LSWI) by combining the shortwave infrared (SWIR) and near-infrared (NIR) data to identify water bodies in MODIS images. Lu *et al.* (2011) recommended an integrated water body extraction technique with HJ-1A/B satellite imagery by utilizing differences between NDVI and NDWI. These modified indices have been commonly used to map surface water bodies using Landsat and MODIS images (Zhong *et al.*, 2008; Li *et al.*, 2009; Soti *et al.*, 2009). However, because of the complexity of cryospheric environment, various surface targets may have the same spectrum characteristics. Therefore, only one type of index method can extract water bodies under certain conditions only (Jawak and Luis, 2013a and 2013b). Additionally, these spectral indices were developed for well-known visible near-IR (VNIR) and shortwave infrared (SWIR) systems. The WorldView-2 (WV-2) provides a duplet of VNIR bands, which offers an opportunity to adapt a novel set of NDWI using eight bands. The present study differs from previous studies by reconstructing the NDWI for 8-band WV-2 data in order to semi-automatically extract lake features.

Spectral processing-based or matching-based feature identification methods, such as Matched Filtering (MF), Mixture Tuned Matched Filtering (MTMF), Spectral Angle Mapper (SAM), MF/SAM ratio, and Principal Component Analysis (PCA), have been implemented for improved mapping and classification of remote sensing images (Peterson *et al.*, 2011; Williams and Hunt, 2002; Boardman, 1998; Kruse *et al.*, 1993; Jia and Richards, 1999). Supervised target detection methods, such as Constrained Energy Minimization (CEM) (Chang *et al.*, 2000), Adaptive Coherence Estimator (ACE) (Bourennane *et al.*, 2011), Target-Constrained Interference-Minimized Filter (TCIMF) (Ren and Chang, 2010), Mixture Tuned TCIMF

Polar Remote Sensing Department, National Centre for Antarctic and Ocean Research (NCAOR), Earth System Sciences Organization (ESSO), Ministry of Earth Sciences (MoES), Government of India, Headland Sada, Goa 403804, India (shridhar.jawak@ncaor.gov.in; shridhar.jawak@gmail.com).

(MT-TCIMF) (Jin *et al.*, 2009), and Orthogonal Subspace Projection (OSP) (Harsanyi and Chang, 1994) methods have been used to improve semiautomatic target detection methods and the classification of multispectral image data. However, comparative studies of these methods have not yet been done on multiband WV-2 data in cryospheric environment for semiautomatic target extraction.

To our knowledge, almost all of the published studies on extraction of surface lakes in cryospheric environments have used satellite remote sensing data. Interestingly, most of the work has focused on extracting only supraglacial lake information, specifically on the Greenland ice sheet (Box and Ski, 2007; Sneed and Hamilton, 2007; Sundal *et al.*, 2009; Tedesco and Steiner, 2011). Cryospheric lake features have been researched primarily by means of multispectral satellite images from the Advanced Spaceborne Thermal Emission and Reflection Radiometer (ASTER) (Lüthje *et al.*, 2006; McMillan *et al.*, 2007), Landsat-7 (Lampkin and VanderBerg, 2011), and MODIS imagery (Selmes *et al.*, 2011).

An accurate manual delineation of lake extent is used (Tedesco and Steiner, 2011; McMillan *et al.*, 2007) when lakes are easily identifiable on images. Applications of methods that discriminate water from surrounding ice and snow is possible on optical images using semiautomatic methods which employ different spectral bands of the satellite sensors (Box and Ski, 2007; Sneed and Hamilton, 2007; Sundal *et al.*, 2009). Many studies have explored methods for semiautomatic or automatic lake feature extraction using medium and coarse resolution satellite remote sensing data (Selmes *et al.*, 2011; Johansson and Brown, 2013). Automated or semi-automated methods have the advantage of rapidly extracting lakes from multitemporal images with large areal coverage (Selmes *et al.*, 2011).

From the literature review (Box and Ski, 2007; Sneed and Hamilton, 2007; Sundal *et al.*, 2009; Tedesco and Steiner, 2011; Lüthje *et al.*, 2006; McMillan *et al.*, 2007; Lampkin and VanderBerg, 2011; Selmes *et al.*, 2011; Johansson and Brown, 2013), it was found that the current methods available for extracting surface lake features in cryospheric environments suffer from the following drawbacks. First, most of these methods are developed and evaluated for the Arctic and Greenland environment and to our knowledge, these methods are not validated for the Antarctic environment. Second, most of these methods have been developed for extracting supraglacial lake features from cryospheric environments, which may not be suitable for extracting the landlocked lakes of the Antarctic, e.g., lakes found in coastal Antarctic oases. Third, most of these studies utilized either medium or coarse resolution optical satellite remote sensing data. As the spatial resolution of an image increases, it is possible to detect smaller lakes. Fourth, to our knowledge, there is no automatic or semiautomatic lake feature extraction method that uses very high resolution satellite remote sensing data for the Antarctic environment. Hence, we present the first comprehensive study on a semiautomatic lake feature extraction approach developed using very high resolution WV-2 data in the Antarctic oasis environment.

The WV-2 satellite offers images at a spatial resolution of 0.50 m in the panchromatic (PAN) band and 2 m in the multispectral (MS) bands, with an average revisit time of 1.1 days. WV-2 MSI consists of four traditional bands, consisting of Band 2, blue (450 to 510 nm); Band 3, green (510 to 580 nm); Band 5, red (630 to 690 nm); and Band 7, near-IR1 (NIR1) (770 to 895 nm), and four new bands: Band 1, coastal (400 to 450 nm); Band 4, yellow (585 to 625 nm); Band 6, red edge (705 to 745 nm); and Band 8, near-IR2 (NIR2) (860 to 1040 nm), which are not available on other commercial platforms. With the aim to provide new techniques for using the WV-2 data, we propose a customized NDWI approach wherein each ratio consists of at least one new or add-on band from the WV-2 MS image.

In this work, we performed semiautomatic extraction of lakes in the Larsemann Hills, Antarctica, by employing three types of pixel-wise approaches: (a) a customized NDWI approach, (b) a spectral processing or matching approach, and (c) a target detection approach. Our experiment focused on the following objectives: (a) designing a customized NDWI approach to extract lake features, (b) comparing the performance of supervised feature extraction algorithms with the newly developed customized NDWI approach using visual analysis and statistical accuracy, and (c) assessing the distinctive 8-band acquisition capability of WV-2 data by performing manifold semiautomatic extraction approaches to compare their reliability in lake area extraction.
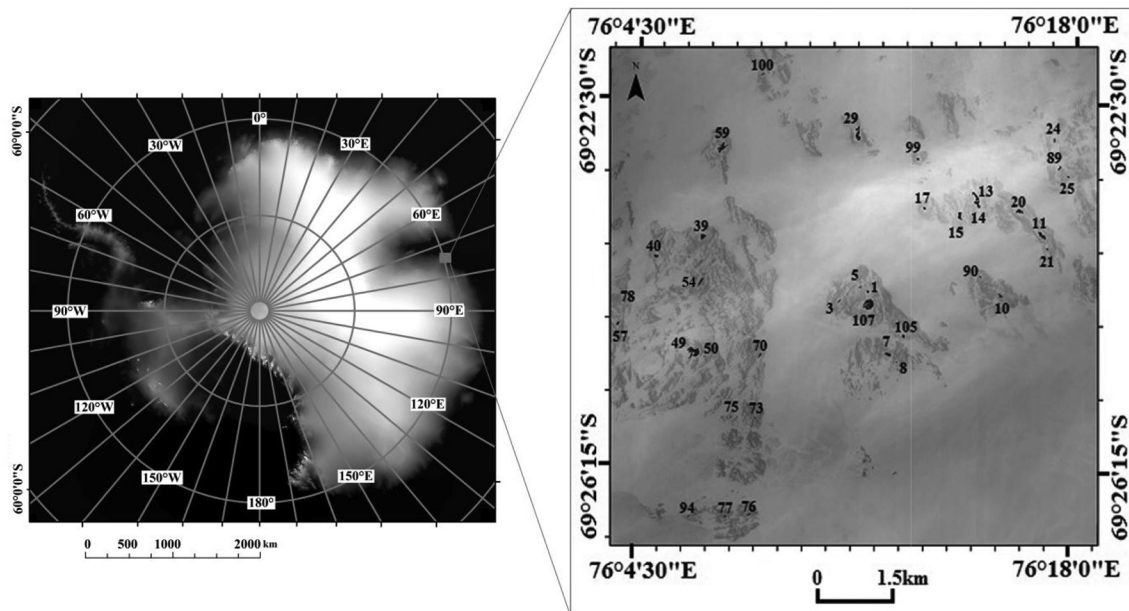

Figure 1. Map of the study area (WorldView-2 PAN imagery) showing the spatial distribution of the 36 lakes under consideration.

Study Area and Data

Study Area

The Larsemann Hills (69°20'S to 69°30 S; 75°55'E to 76°30'E) are located on the Ingrid Christensen Coast, Princess Elizabeth Land, east Antarctica. The region is a typical ice-free Antarctic coastal oasis with a series of low rounded exposed rocks and low rolling hills along the southeast shore of Prydz Bay. The region hosts a number of small lakes, ranging from small, shallow ponds (<1 m deep) to large glacial lakes such as Progress lake (~38 m deep), with areas ranging between 100 m² and 33,000 m². In winter, some of these lakes are covered by 2 m thick ice, while others remain ice-free for succinct phases or moderately ice-free throughout the austral summer (September to February) when water temperatures increase to 8°C in a few of the surface water bodies. Most lakes are mainly fed by fresh snowfall and glacial melt water. The WV-2 image of the Larsemann Hills (Figure 1) covers an area of approximately 100 km² with different land cover features such as snow, ice, exposed rocks, lake features, permafrost, etc.

Satellite Data

We employed radiometrically corrected, georeferenced, ortho-rectified 16-bit standard level 2 (LV2A) WV-2 multi-sequence data. The data was composed of nine cloud-free image strips consisting of 8-band MSI and PAN images acquired on 10 September 2010, over the Larsemann Hills in Antarctica. A total of nine strips were geospatially fused by mosaicking process to create a single continuous WV-2 image.

Description of Reference and Manually Digitized Map Dataset

The ground reference datasets utilized to support the semiautomatic extraction of lakes were retrieved from the Australian Antarctic Data Centre (AADC), Indian Scientific Expedition to Antarctica (InSEA), historical Google Earth® images, and PAN-sharpened WV-2 images (Table 1). Extensive field surveys have already been carried out by the AADC over the last few decades (*http://www.aad.gov.au/*) and by teams participating in the InSEA since 2005. One important dataset of the land cover map for the Larsemann Hills was produced by AADC (Harris, 2002) which is titled *Larsemann Hills Photogrammetric Mapping Project*. Additionally, AADC's collection of geographical information system (GIS) layers, such as contours, geological structures, water bodies, etc., were used as supplementary datasets to generate our reference map.

A geodatabase consisting of 110 randomly distributed lakes in the Larsemann Hills region was generated by manual digitization. PAN-sharpened images (0.5 m) were visualized in ArcGIS® 10 at several scales using various band combinations: 742, 872, 632, 532, and 732. However, we could easily recognize the shoreline, shape and size (dimension) of lake features along with better visualization and discrimination of lake features against background features using 532 band combination and 1:500 scale. Hence, we selected a 1:500 scale and the 532 band combination for digitization of the lake features. Each lake polygon was then edited to eliminate digitization errors.

Quality control involved cross-checking the lake feature boundaries to ensure accurate and consistent interpretation and digitization. Then, the positional accuracy of the digitized lake database was calculated using an independent source of eight accurate differential global positioning system (DGPS) point locations (Congalton, 2008; Congalton and Green, 1999; Congalton, 1991). The root mean square error (RMSE) of digitization yielded ≈25 mm (less than one pixel) when compared with the DGPS source. The manually digitized lakes were extensively surveyed, confirmed and cross-checked using DGPS ground reference data obtained from field campaigns, AADC maps, and Google® images.

A field survey of 50 lakes was carried out in the real-time-kinematic (RTK) mode with a positional accuracy of ≈10 mm using the Leica Viva DGPS surveying unit. Since these field datasets were collected from 2008 to 2012 (September to February), they were processed to conform the 2010 (September)

TABLE 1. A LIST OF SATELLITE AND GROUND REFERENCE DATASETS AND THEIR SPECIFIC USAGE IN THIS STUDY FOR EFFECTIVE LAKE FEATURE EXTRACTION

Dataset	Source	Temporal range	*Utilization of datasets in the context of present study				
(dd/mm/yy)			1) Semi-automatic extraction	2) Visual interpretation	3) Manual digitization	4) Supplementing digitization	5) Digitization error analysis
Worldview-2 MSI (2 m) and PAN (0.5 m)	Digital-Globe	10/09/2010	✘	✔	✘	✔	✘
Worldview-2 PAN-sharpened image (0.5m)	Processed	10/09/2010	✔	✔	✔	✔	✔
Google earth Images	Google	31/12/1999 24/02/2006 03/03/2006 04/01/2011	✘	✔	✘	✔	✘
GIS Layers from Landsat Image	AADC	30/01/2002	✘	✔	✘	✔	✘
Land cover Map (1:2500)	InSEA	2007-2008 (September to March)	✘	✔	✘	✔	✘
DGPS Surveying	InSEA	2008-2011 (September to March)	✘	✔	✔	✔	✔

*A variety of spatial datasets (both satellite data and ground reference data) were utilized at different stages of the present study to accomplish various tasks. The potential usage of these datasets includes: 1] For semiautomatic feature extraction: The datasets are used as input for semiautomatic extraction methods, 2] For visual interpretation: The datasets are used for visual interpretation to support digitization, to interpret lake shorelines, and to ensure spatial snow/ice cover changes, 3] For manual digitization: The datasets are essentially used in ArcGIS platform to carry out digitization, 4] For supplementing digitization: The datasets are used to cross-check and verify the manual digitization against various ground reference and satellite images, and 5] For digitization error analysis: The datasets are used to test the positional errors in manual digitization. (✔ denotes "Yes or used" and ✘ denotes "No or not used")

images. Careful visual examination was conducted to eliminate those samples that were not present in the existing WV-2 imagery because they may have been completely frozen. Additionally, only 44 lakes mapped during September to December corresponding to the WV-2 image acquisition date (10 September 2010) were considered in the present analysis in order to reduce the errors associated with temporal changes in shoreline geometry. Those 44 lakes mapped using DGPS during September to December were overlaid on the WV-2 PAN-sharpened image and checked against the digitized reference database consisting of 110 lakes. After a careful visual analysis, eight manually digitized lakes that had higher boundary variations (typically greater than 1 pixel, i.e., 50 cm) compared with the ground surveyed lake boundary were eliminated. Finally, only 36 lakes (out of 110) extracted by manual digitization and confirmed by the DGPS survey were considered in the present analysis (Figure 1). A GIS-compatible shapefile of the lakes was generated using ArcGIS 10. The surface area of all 36 lakes was calculated using GIS routines. A list of the 36 lakes and their reference areas are summarized in Table 2.

Methodology

The data processing protocol is shown in Figure 2. The steps consist of three blocks: (a) data preprocessing, (b) PAN-sharpening and feature extraction, and (c) quantitative evaluation. Each block of the methodology (Figure 2) is discussed below.

Data Preprocessing

Two procedures were implemented for data preprocessing: (a) dark object subtraction (DOS) and (b) data calibration.

Dark Object or Pixel Subtraction (DOS)

The DOS was performed to reduce the path radiance from each band in order to evenly spread the data values in space with regard to a dynamic range. Following the literature (Chavez, 1996), we used clear water bodies as dark objects.

Data Calibration

The calibration method was adapted from literature (Updike and Comp, 2010). The calibration procedure was carried out in two steps: (a) conversion of the raw digital number values to at-sensor spectral radiance factors, and (b) conversion from spectral radiance to Top-of-Atmosphere (TOA) reflectance.

PAN-Sharpening and Feature Extraction:

PAN-Sharpening

The 8-band image was PAN-sharpened from a spatial resolution of 2.00 m to 0.50 m to create an image of 0.50 m spatial resolution. Among the hundreds of PAN-sharpening algorithms available for remote sensing applications, we used the five most popular and effective algorithms for feature extraction. These algorithms are Principal Component Analysis (PCA) (Chavez et al., 1991), Brovey's Transform (BT) - Resolution Merge (Hallada and Cox, 1983), Wavelet-based Principle Component (W-PC) (Pradhan et al., 2006), Ehler's Fusion (EF) (Klonus and Ehlers, 2007), and Gram Schmidt (GS) (Laben et al., 2005). We selected these methods because they yield less spectral distortion than other fusion methods, such as IHS (Zhang, 2002). Since the PAN and MSI images were acquired by the sensor at the same time, PAN-sharpening process was performed directly without supplementary registration.

Feature Identification and Extraction

This procedure consisted of three semiautomatic feature extraction approaches: (a) a customized NDWI approach, (b) a spectral processing approach, and (c) a target detection approach.

TABLE 2. SAMPLE DATA SUMMARIZING THE REFERENCE AREA (MANUALLY DIGITIZED) FOR THE 36 LAKES AND THEIR RESPECTIVE EXTRACTED AREAS BY THE CUSTOMIZED NDWI APPROACH USING GS-SHARPENED IMAGES; 11 PARTIALLY ICE/ SNOW-COVERED LAKES WERE FOUND IN THE STUDY AREA, WHICH ARE HIGHLIGHTED WITH GREY SHADING

Sr. No.	Reference Data		NDWI$_{(1-8/1+8)}$	NDWI$_{(2-7/2+7)}$	NDWI$_{(1-7/1+7)}$	NDWI$_{(2-8/2+8)}$
	Lake Number	Reference Area(m²)	Extracted Area(m²)	Extracted Area(m²)	Extracted Area(m²)	Extracted Area(m²)
1	1	1756.77	1740.79	1734.77	1693.80	1735.77
2	3	1142.40	1126.46	1121.35	1222.36	1193.10
3	5	906.85	972.63	867.28	872.01	868.02
4	7	5733.07	5995.04	5006.45	5970.20	5730.17
5	8	434.61	531.81	532.73	473.52	478.63
6	10	2896.46	2742.04	2812.09	2730.09	2777.18
7	11	8555.20	8008.25	8664.75	8592.75	8182.65
8	13	7064.52	7612.05	7005.11	6666.38	6663.81
9	14	7060.11	7287.18	6812.95	6857.95	6875.14
10	15	6852.28	6663.88	7055.56	6365.39	7098.68
11	17	1432.61	1409.59	1669.80	1344.65	1273.28
12	21	985.25	1254.25	1049.90	1157.59	1006.86
13	24	1467.05	1402.50	1472.88	1494.75	1403.54
14	25	980.63	856.38	956.38	892.75	841.15
15	29	12653.63	12213.12	12075.65	12283.15	12601.85
16	39	7538.12	7327.16	7049.70	7380.23	7370.49
17	40	3919.99	3992.93	3980.72	3974.83	3945.18
18	49	25003.67	25055.68	25716.15	25028.71	25308.21
19	50	379.68	487.48	328.07	369.87	349.07
20	54	2458.37	2428.24	2469.62	2405.06	2489.83
21	57	2457.17	2401.31	2492.78	2485.34	2490.27
22	59	14369.53	14255.44	14060.77	14782.87	14277.43
23	70	778.98	661.93	629.29	623.91	779.78
24	73	866.40	1023.96	916.52	1067.94	944.26
25	75	374.25	547.90	424.24	403.78	352.92
26	76	1945.61	1950.75	1969.40	1994.35	1813.32
27	77	1429.51	1475.21	1487.96	1405.92	1487.59
28	78	190.82	149.36	172.23	156.16	213.93
29	80	289.66	301.20	320.77	388.09	264.69
30	89	1959.18	1998.00	1900.38	1976.75	1922.73
31	90	944.80	874.77	1065.07	978.88	758.43
32	94	1098.58	1198.44	1127.16	1152.23	1176.46
33	99	1302.80	1425.46	1194.42	1439.86	1314.35
34	100	1125.59	1275.24	1236.42	1226.07	1072.82
35	105	2770.54	2880.86	2859.29	2694.04	2814.66
36	107	33032.76	33721.30	33274.89	33136.48	33883.65

a) Customized NDWI Approach

Most of the existing NDWIs make use of the SWIR, green, and NIR bands to highlight surface water bodies (McFeeters, 1996; Lacaux et al., 2007; Xu, 2005; Xiao et al., 2005). However, for WV-2 data, the NDWIs were recreated to incorporate the new bands and design customized NDWIs for lake extraction. Hence, in addition to existing NDWI, we propose various modifications or customized NDWIs in this study to fully utilize the add-on WV-2 bands. Our unique set of customized NDWIs was designed using the spectral responses of various lakes present on the WV-2 image.
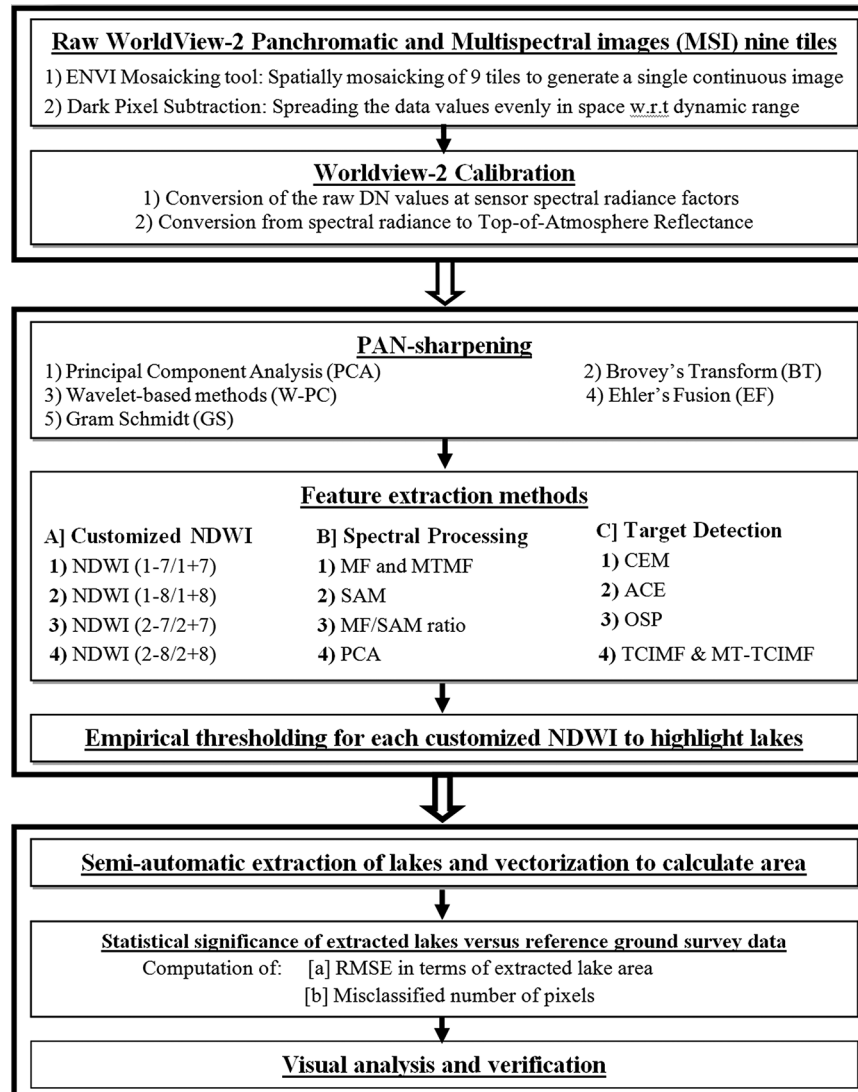
Raw WorldView-2 Panchromatic and Multispectral images (MSI) nine tiles
1) ENVI Mosaicking tool: Spatially mosaicking of 9 tiles to generate a single continuous image
2) Dark Pixel Subtraction: Spreading the data values evenly in space w.r.t dynamic range

Worldview-2 Calibration
1) Conversion of the raw DN values at sensor spectral radiance factors
2) Conversion from spectral radiance to Top-of-Atmosphere Reflectance

PAN-sharpening
1) Principal Component Analysis (PCA)   2) Brovey's Transform (BT)
3) Wavelet-based methods (W-PC)   4) Ehler's Fusion (EF)
5) Gram Schmidt (GS)

Feature extraction methods

A] **Customized NDWI**   B] **Spectral Processing**   C] **Target Detection**
1) NDWI (1-7/1+7)   1) MF and MTMF   1) CEM
2) NDWI (1-8/1+8)   2) SAM   2) ACE
3) NDWI (2-7/2+7)   3) MF/SAM ratio   3) OSP
4) NDWI (2-8/2+8)   4) PCA   4) TCIMF & MT-TCIMF

Empirical thresholding for each customized NDWI to highlight lakes

Semi-automatic extraction of lakes and vectorization to calculate area

Statistical significance of extracted lakes versus reference ground survey data
Computation of: [a] RMSE in terms of extracted lake area
                    [b] Misclassified number of pixels

Visual analysis and verification

Figure 2. Experimental protocol for semiautomatic extraction of lake information.

In this study, customized NDWIs were experientially estimated through repetitive and robust spectral profile observations. We identified the most useful bands for discriminating lakes by visual inspection. Each NDWI was computed by comparing the relative responses of various lakes in the spectral space. The spectral bands were ordered or ranked for maximum and minimum response values for lakes; bands were also ordered using the minimum redundancy maximum relevance (mRMR) principle (Peng *et al.*, 2005). Lake regions in the MS image were selected and then a combination of spectral bands that prominently discriminated the lake features was obtained. Nearly 300 spectral profiles from the 36 lakes were evaluated to ensure the maximum and minimum response band for the lake class. These bands were normalized to yield a customized NDWI for effective semiautomatic lake extraction (Table 3).

Traditionally, the blue band is normalized to the NIR band (Huggel, 2002; Xie *et al.*, 2013), since the distinction in spectral response is clearly evident. In this study, the coastal band was normalized to the NIR2 band, since the difference of each of these bands

TABLE 3. CUSTOMIZED SPECTRAL INDEX RATIOS DEVISED AS AN EFFECTIVE SEMIAUTOMATIC EXTRACTION TOOL FOR SURFACE LAKE FEATURES

Normalized Difference Water Index	Mathematical Expression
NDWI$_{(1-7/1+7)}$	$\dfrac{Coastal - NIR1}{Coastal + NIR1}$
NDWI$_{(2-7/2+7)}$	$\dfrac{Blue - NIR1}{Blue + NIR1}$
NDWI$_{(1-8/1+8)}$	$\dfrac{Coastal - NIR2}{Coastal + NIR2}$
NDWI$_{(2-8/2+8)}$	$\dfrac{Blue - NIR2}{Blue + NIR2}$

provided an enhanced contrast and produced a distinct threshold for detecting regions of standing water. Because there are no buildings in the Larsemann Hills that have an analogous spectral response to water and

PAN-sharpening	NDWI$_{(1-7/1+7)}$	NDWI$_{(1-8/1+8)}$	NDWI$_{(2-7/2+7)}$	NDWI$_{(2-8/2+8)}$
GS	0.6451-0.6722	0.6489-0.6630	0.6713-0.7457	0.6681-0.6941
PC	0.6887-0.7119	0.6608-0.6862	0.7419-0.7712	0.7138-0.6745
Wavelet-PC	0.7193-0.7329	0.6990-0.7190	0.7713-0.7948	0.7695-0.8049
EF	0.7364-0.7634	0.7223-0.7345	0.7948-0.8305	0.8176-0.8362
BT	0.7686-0.7885	0.7510-0.7726	0.8310-0.8737	0.8345-0.8679

because the satellite data was captured with minimum cloud cover, the standing water was the only target that appeared bright on the NDWI image. However, the NDWI does not imply a maximization of the spectral response of a particular feature, but rather it gives a better discrimination of the lake class over other classes in the image. This means that in a specific range of values defined by threshold, NDWI contains a certain water class. Thereafter, the customized NDWIs were calculated against the values in the radiance cube, and an output image was generated for each customized NDWI.

The WV-2 image data was captured during the beginning of the austral spring when solar radiation reaches the surface and initiates ice melting in Antarctica. This led to a similar spectral response of NDWI for melt water on the surface of snow and in lakes, since NDWI discriminates water from other land cover features. To discriminate between melt water on the surface of snow and on lakes, it was essential to threshold the NDWI value so that the entire region was classified as the target class (lakes) or a non-target class (snow, rocks, and melt water).

Since the lake areas exhibited NDWI values ranging from 0.64 to 0.86, a scene-dependent threshold was defined and used to discriminate between lake and non-lake pixels. Threshold values used in this study were empirically evaluated by manually scrutinizing the most obvious 300 lake pixels from the NDWI images obtained from the PAN-sharpened images. Analyses were performed at the same pixel locations for all NDWI images derived from PAN-sharpened images to verify unbiased accuracy analysis. A list of the thresholds defined for the customized NDWI methods are summarized in Table 4. Pixels with higher NDWI value than the local threshold were coded as 1 (target lake class pixels), while pixels with a lower NDWI value were coded as 0 (non-target class pixels). After classifying the image based on each customized NDWI, the 36 semi-automatically extracted lakes were vectorized to calculate the area of individual lake.

b) Spectral Processing or Matching-based Extraction Approach

Spectral matching methods extract the target features that are depicted in multispectral imagery based on the target feature's spectral characteristics. The supervised workflows require an initial approximation in terms of regions of interest (ROIs) as reference spectra or seed points that include representative pixels of the desired target class. Spectral matching algorithms determine the spectral similarity or matching between input satellite imagery and reference seed points to create an output product in which pixels with similar spectral properties are clumped into target and non-target classes.

The Spectral Processing Exploitation and Analysis Resource (SPEAR) workflow tools and mapping methods (ENVI 4.8) were utilized, which streamline spectral processing methods (MF, MTMF, SAM, MF/SAM ratio, and PCA) for mapping open and obscured water bodies using WV-2 PAN-sharpened data. Lakes covered with snow showed a wide range of turbidity, ranging from light blue or green to almost black. The major influences came from sediment influx, water depth, topography of the lake bottom, and the origin of the lake water (Wessels, 2002). Because of this difference in spectral information, unsupervised classification methods were not used for automated lake mapping. Since one of our objectives was to extract lake features semi-automatically, we processed the image using supervised workflows based on the knowledge of water locations within the landscape.

c) Target Detection Approach

Target detection algorithms work on the principle of extracting target features based on spectral characteristic of initial training spectral signatures of target features, and suppressing the background noise using spectral signatures of non-target features. These algorithms provide a rapid means to maximize the response of the known target spectra and suppress the response of the composite unknown background targets. The initial approximations or spectral signatures for supervised workflows are provided in terms of target ROIs and non-target ROIs.

Target detection tools (ENVI 4.8) were executed to perform supervised image processing tasks into workflows (CEM, ACE, OSP, TCIMF, and MT-TCIMF) to extract lake features. We referred to the target detection workflow introduced by Jin *et al.* (2009) that couples a Minimum Noise Fraction (MNF) transform for improved target detection. The use of a MNF transform improves the target detection for multispectral data (Jin *et al.*, 2009). Additionally, for MT-TCIMF, the MNF transformed image fuses the mixture-tuned method with the TCIMF method. Hence, the MNF was used to resolve the intrinsic spectral dimensionality of the WV-2 image to support subsequent processing (Jin *et al.*, 2009). The MNF transformation served two purposes: (a) MNF was used to extract target features and/or reduce dimensions for the generic target detection methods, such as ACE, CEM, and OSP; and (b) For the mixture tuned method (MT-TCIMF), applying the MNF transform resulted in the isotropic variance noise, which was used to compute infeasibility value. By adding an additional infeasibility band, mixture tuned techniques improved the detection results by reducing the number of false spectral signals.

The feature extraction methods described in this section are based on different underlying principles. Hence, to compare these methods objectively, we kept the input ROIs (regions of interest or training samples) constant for all methods. After classifying the image into target spectra, i.e., lakes, using the spectral processing or target detection approaches, the 36 semi-automatically extracted lakes were vectorized to calculate the area of individual lake.

Accuracy Assessment
A pre-digitized geodatabase of lake areas of the 36 extracted lakes in the form shapefiles was

Feature extraction methods		PAN-sharpening methods					
Customized NDWI	*References*	Wavelet-PC	BT	PC	GS	EF	Average
NDWI$_{(1-7/1+7)}$	*Present work*	*197.169*	219.419	*215.069*	273.793	243.610	**229.812**
NDWI$_{(1-8/1+8)}$	*Present work*	240.678	226.682	*216.425*	220.945	232.062	**227.358**
NDWI$_{(2-7/2+7)}$	*Present work*	199.409	265.034	244.917	***173.540***	257.935	**228.167**
NDWI$_{(2-8/2+8)}$	*Present work*	256.736	249.119	225.674	*206.053*	238.719	**235.260**
	Average RMSE	**223.498**	**240.064**	**225.521**	**218.583**	**243.081**	**230.149**
Spectral Processing							
MF	*Williams and Hunt (2002)*	253.346	253.071	237.355	*232.220*	258.748	246.948
MTMF	*Boardman (1998)*	212.170	**203.606**	**181.459**	237.700	243.382	215.663
SAM	*Kruse et al. (1993)*	*224.525*	266.646	289.736	256.914	248.709	257.306
MF/SAM	*Peterson et al. (2011)*	240.147	244.484	250.085	*221.937*	272.012	245.733
PCA	*Jin et al. (2009)*	253.071	*211.106*	229.177	219.690	266.092	235.827
	Average RMSE	**236.652**	**235.783**	**237.562**	**233.692**	**257.789**	**240.296**
Target Detection							
CEM	*Chang et al.(2000)*	221.572	278.534	200.658	258.289	***170.814***	**225.973**
ACE	*Bourennane et al. (2011)*	220.949	249.119	223.125	*199.866*	209.559	**220.524**
OSP	*Harsanyi and Chang (1994)*	251.852	*213.393*	269.316	215.447	276.204	**245.243**
TCIMF	*Ren and Chang (2010)*	***165.001***	282.675	210.604	242.737	214.512	**223.106**
MT-TCIMF	*Jin et al. (2009)*	211.652	206.748	245.191	*182.904*	197.210	**208.741**
	Average RMSE	**214.205**	**246.094**	**229.779**	**219.849**	**213.660**	**224.717**
Total average (RMSE) in m²		**224.877**	**240.688**	**231.342**	**224.431**	**237.826**	

utilized as reference for assessing the accuracy of the semiautomatic extraction methods. Using the vectorized outputs from the extraction procedures, the areas of the extracted lakes were estimated and area statistics were compared with lake areas in the manually digitized database. For quantifying the uncertainty of our analysis, we used the root mean square error (RMSE), because it is a more consistent and statistically significant indicator of accuracy. Mathematically, RMSE is expressed as:

$$RMSE = \sqrt{\frac{1}{n} \sum_{i-1}^{n} \left(Ar_i - Am_i \right)^2} \tag{1}$$

where Am_i is the ith original area value measured using the semiautomatic extraction method, Ar_i is the corresponding value measured on the reference ground surface, and n is the number of lakes, corresponding to the sample size of the dataset.

Bias for each extracted lake is defined as:

$$Bias = A_{reference} - A_{measured} \tag{2}$$

where, $A_{reference}$ is the lake area obtained from ground reference data, and $A_{measured}$ is the area calculated from semiautomatic extraction method. A positive (negative) bias value indicates an average amount of underestimation (overestimation) in the area.

For any semiautomatic extraction method, total misclassified area (m²) can be calculated by summation of all absolute bias values (independent of positive or negative sign) for 36 lakes, as follows:

$$\text{Total misclassified area (m}^2) = \sum_1^{36} \text{Abs (Bias)} \tag{3}$$

where, Abs (Bias) is the absolute positive values of bias (m²) for all the 36 lakes for a particular semiautomatic extraction method under consideration.

The total misclassified area, overestimated area, and underestimated area can also be expressed in terms of percentage, as follows:

$$\text{Total misclassified area (\%)} = \frac{\sum_1^{36} \text{Abs} \left(\text{Bias} \right)}{\sum_1^{36} A_{reference}} \times 100 \tag{4}$$

$$\text{Total underestimated area (\%)} = \frac{\sum \text{Positive Bias}}{\sum_1^{36} A_{reference}} \times 100 \tag{5}$$

$$\text{Total overestimated area (\%)} = \frac{\sum \text{Abs} \left(\text{Negative Bias} \right)}{\sum_1^{36} A_{reference}} \times 100 \tag{6}$$

where, $\sum_1^{36} A_{reference}$ is the summation of areas obtained from ground reference data for 36 lakes, $\sum$ Positive Bias is the summation of all positive bias values (out of 36 lakes) produced by semiautomatic extraction method, and $\sum$ Abs (Negative Bias) is the summation of absolute (positive) values of all the negative biases produced by semiautomatic extraction method.

Experimental Results

Approaches for Semi-automatic Extraction of Lakes
The average RMSE for each PAN-sharpening algorithm (row) and each extraction method (column) was calculated to comment on overall stability and consistency of the respective algorithm (Table 5). In addition, local RMSE averages for each extraction method were calculated to assess the performance of each method within a respective extraction approach. Sample data used in RMSE calculations for GS-sharpened images using the customized NDWI approach are shown in Table 2.

We analyzed semiautomatic feature extraction approaches for delineation of lakes, which were categorized as (a) the customized NDWI approach (average RMSE = 230.149 m^2), (b) the spectral processing approach (average RMSE = 240.296 m^2), and (c) the target detection approach (average RMSE = 224.717 m^2). Our experiment revealed that existing target detection approach outperformed the other approaches used with the five PAN-sharpening algorithms. The customized NDWI approach was intermediate between the other two approaches. The overall reliability of all the extraction methods within the respective approaches was based on the RMSE values and is discussed below. The variation in RMSE between the three approaches is summarized in Table 5.

Performance of the Target Detection Approach
Among the five target detection methods applied to the five PAN-sharpened WV-2 images, the MT-TCIMF outperformed the other methods, while OSP performed the worst in extracting lake features (Table 5, Average RMSE). ACE delivered better results than TCIMF and CEM, but the difference in average RMSE for ACE, CEM, and TCIMF was found to be comparable in a given cohort. Surprisingly, the performance of OSP was found to be worse than that of the customized NDWI approach.

Performance of the Customized NDWI Approach
The NDWI$_{(1-8/1+8)}$ combination yielded superior results, while NDWI$_{(2-8/2+8)}$ produced inferior results, compared to the remaining two combinations in a group of four practiced NDWIs (Table 5, Average RMSE). On other hand, the differences in average RMSE for NDWI$_{(1-7/1+7)}$ (229.812 m^2), NDWI$_{(1-8/1+8)}$ (227.358 m^2), and NDWI$_{(2-7/2+7)}$ (228.167 m^2) seemed comparatively negligible in a given group. The customized NDWI approach was found to be superior to the spectral processing approach and inferior to the target detection approach. Overall, the customized NDWI approach surpassed the accuracy associated with the OSP method of the target detection approach. In general, the performance of this method in terms of average RMSE was found to be intermediate in comparison to the other two methods.

Performance of the Spectral Processing Approach
The MTMF spectral processing method (average RMSE = 215.663 m^2) produced the best results compared with the other methods of this approach. It was the only method in this category that outperformed the customized NDWI approach, while all the other spectral processing methods performed worse than the customized NDWI approach (Table 5, Average RMSE).

The MF/SAM ratio method performed better than its individual components, i.e., SAM and MF, which was expected. The difference in average RMSE between MF/SAM and MF was comparable, which suggests that the poor performance of MF/SAM may be attributed to the overall poor performance of the SAM component. Interestingly, PCA performed significantly better than MF, SAM, and the MF/SAM ratio. In addition, PCA was the only method in this set that exceeded the accuracy of the OSP method (a target detection approach), suggesting that PCA rendered fewer false alarms compared to OSP.

Overall Performance of Semiautomatic Extraction Methods
The overall trend of performance for all the lake extraction methods, based on RMSE, are summarized in Figure 3a and can be ranked as follows: MT-TCIMF > MTMF > ACE > TCIMF > CEM > NDWI$_{(1-8/1+8)}$ > NDWI$_{(2-7/2+7)}$ > NDWI$_{(1-7/1+7)}$ > NDWI$_{(2-8/2+8)}$ > PCA > OSP > MF/SAM > MF > SAM. This order suggests that the methods can be grouped by approach and ranked as follows: target detection approach > customized NDWI approach > spectral processing approach.

The average RMSE values for the customized NDWI approach ranged from ~227 m^2 to ~235 m^2, and for the spectral processing approach and the target detection approach, RMSE values varied from ~215 m^2 to 258 m^2 and from ~208 m^2 to ~246 m^2, respectively (Table 5 and Figure 4). The smallest variation
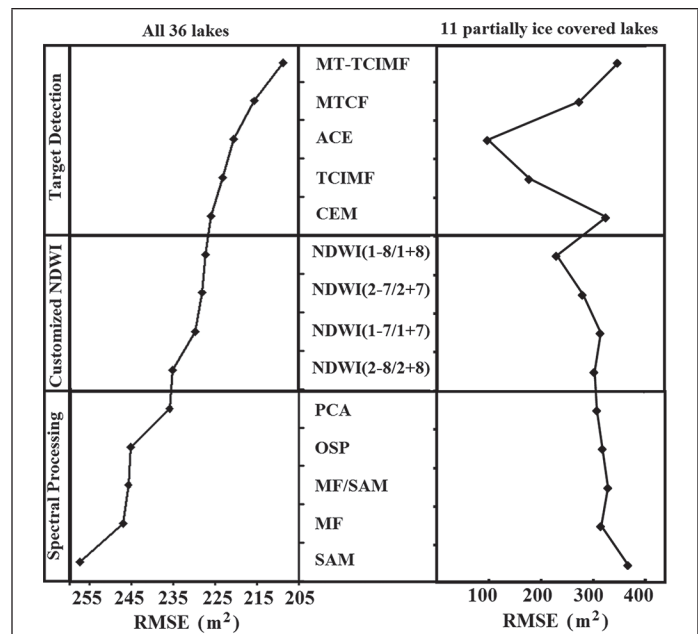

Figure 3. (a) The overall performance trend for all lake extraction methods, in terms of RMSE, and (b) The overall performance of the extraction methods for extracting partially ice/snow-covered lakes, based on RMSE (m^2).
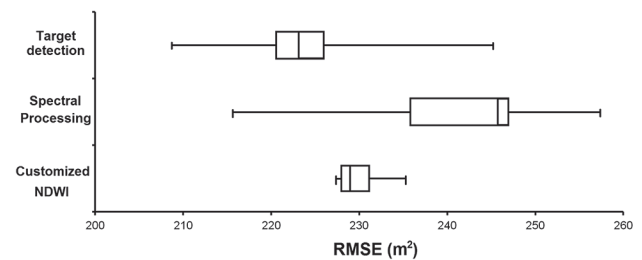

Figure 4. Box plot showing variation of RMSE for three lake feature extraction approaches.

in RMSE was found in the customized NDWI approach, which suggests that it is a more stable and consistent approach than the other two lake extraction approaches. In terms of intra-stability associated with each approach, we rate them as follows: customized NDWI approach > target detection approach > spectral processing approach.

A visual analysis of the four best lake extraction results achieved by the customized NDWI approach is represented in Figure 5. A sample visual comparison of the shoreline of semiautomatically extracted lake feature using the customized NDWI and the manual reference is shown in Figure 6.

The mixed tuned matched filtering methods (MTMF and MT-TCIMF) outperformed the other extraction methods, while the MF and SAM methods were the worst of the 14 extraction methods. In general, mixed tuned methods consistently achieved a minimum number of false alarms for all lakes. Our results also suggest the moderate potential of the NDWI approach in extracting lakes features.

Among all the methods, excluding mixed tuned matched filtering methods, results of the ACE method (RMSE = 220.524 m^2) showed great target visibility and the capability to suppress false signals, resulting in a low RMSE when compared with other methods. In the ACE output image, the target was clearly discriminated from the background when compared to the SAM image (most erroneous), suggesting that the former provides more decisive results than the latter. In our
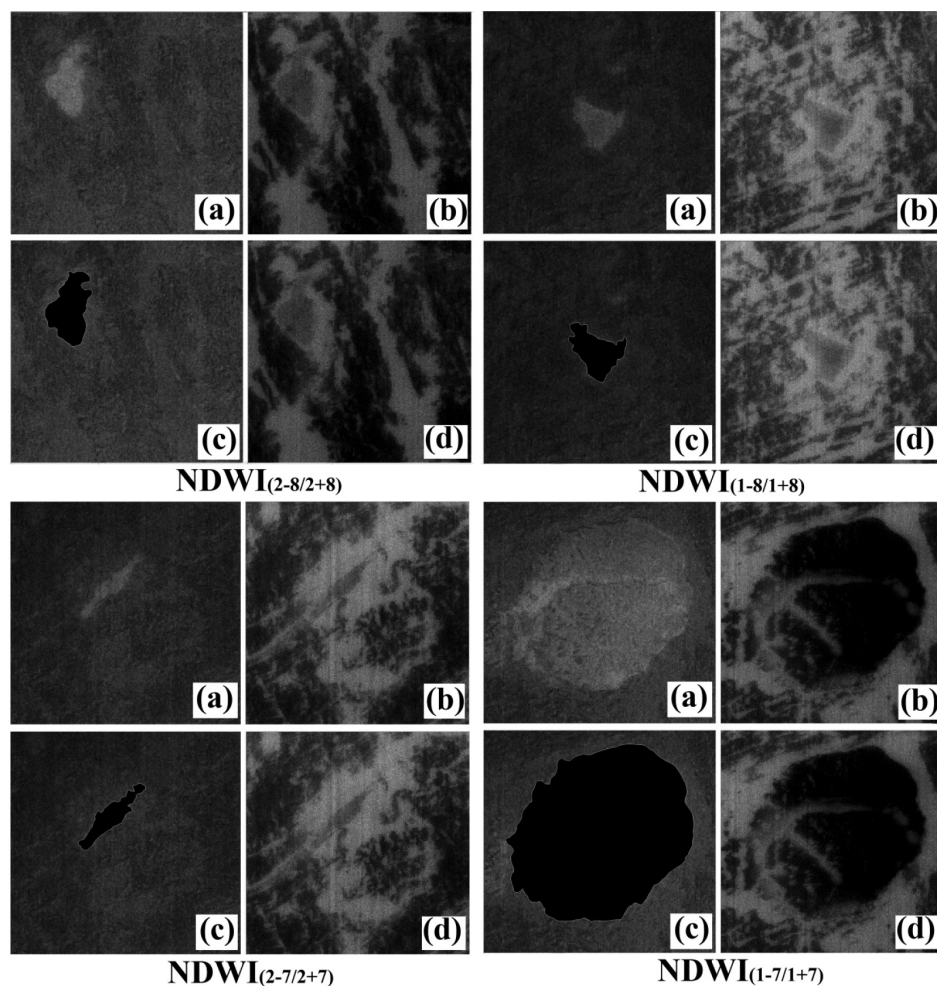
Figure 5. A visual analysis images of the sample four lakes for which best results were obtained using four NDWI methods under customized NDWI approach. For each standalone NDWI method, four images are depicted at 1:1000 scale , namely, (a) NDWI image before thresholding, (c) NDWI image after thresholding with extracted lake feature, with (b) and (d) GS-sharpened multispectral image.
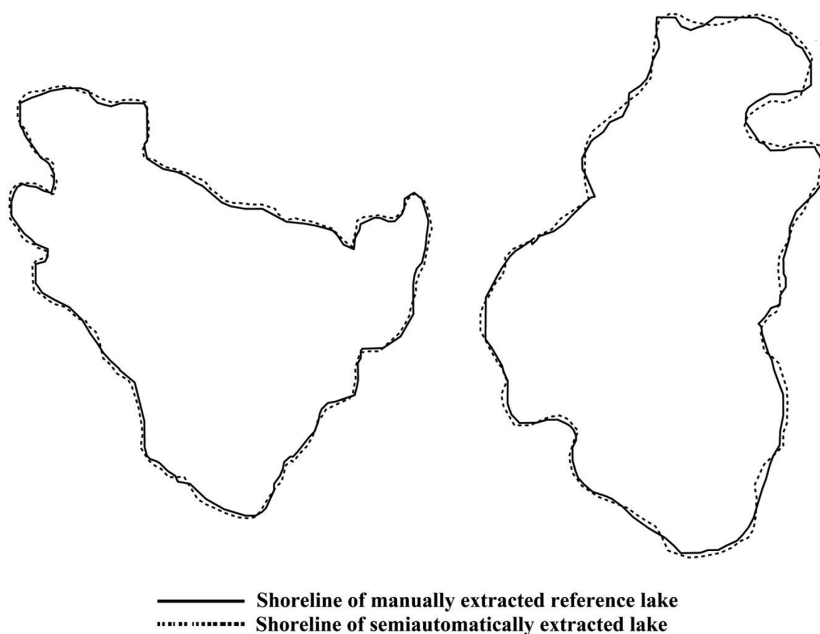

——————— Shoreline of manually extracted reference lake
·······▪········· Shoreline of semiautomatically extracted lake

Figure 6. A sample visual interpretation for customized NDWI based semiautomatically extracted lake features with the manual reference at 1:400 scale. Figure 6a denotes the best case visual comparison, and Figure 6b denotes the worst case visual comparison.

experiment, the ACE method performed better than the other methods by better differentiating the target from the background features. Similar to CEM and MF, ACE provided a rapid means of detecting a specific target signature based on the ROI or signature spectra and did not involve data of all the other spectral signatures within the scene.

The comparative analysis of RMSEs (Table 5) suggests that MT-TCIMF (RMSE = 208.741 m²) was able to greatly reduce the number of false signals compared with MTMF (RMSE = 215.663 m²). In general, TCIMF can be viewed as an extension of the CEM detector. Our results concur with earlier studies, which revealed that if the spectral angle between the target and the non-target is significant, TCIMF can potentially reduce the number of false positives when compared with the CEM method. Based on the RMSEs computed from the number of false alarms, CEM and TCIMF achieved better performances than the customized NDWI approach and the spectral processing approaches.

MT-TCIMF showed the best performance in the cohort, given its average RMSE of 208.741 m², which was the lowest of the 14 extraction methods. The OSP method showed poor lake extraction capabilities (RMSE = 245.243 m²), indicating that it produced many false alarms. However, TCIMF performed significantly better than the customized NDWI methods and the OSP method. Our results suggest that CEM (RMSE = 225.973 m²) and TCIMF (RMSE = 223.106 m²) performed much better than OSP (RMSE = 245.243 m²) when applied to lake extraction from WV-2 data. The outcomes and observations of these semiautomatic extraction procedures as a whole suggest that the target detection approach performed better than the other two approaches analyzed.

We also found that SAM was suitable for lake detection, even though its performance was poor (RMSE = 257.306 m²). The MF/SAM ratio suppressed the false positives that were present when using only one of the methods (MF or SAM) but not when using the other, while enhancing the true positives. For example, if a pixel representing water had a high MF and low SAM value, the ratio (MF/SAM) would produce a high true positive. Conversely, if the MF product had a high value for a false positive, but the SAM would correctly mapped it as a non-water pixel (high value), the ratio of these high values led to a smaller value, which suppressed the false positive. Hence, MF/SAM (RMSE = 245.733 m²) ratio performed considerably better than MF (RMSE = 246.948 m²) and SAM (RMSE = 257.306 m²) alone.

Out of the 36 lakes under consideration, 11 of them were partially covered with ice or snow, which can confound spectral signatures as a result of suspended sediments and variable snow cover. Table 6 presents the RMSE results pertaining only to those 11 lakes, identified as lake number 7, 11, 14, 21, 24, 39, 57, 70, 73, 78, and 89 (bolded lake numbers in Table 2). The overall trend of accuracy for the lake extraction methods as they pertain to snow-covered lakes, based on RMSE, is as follows: ACE > TCIMF > NDWI$_{(1-8/1+8)}$ > MTMF > NDWI$_{(2-7/2+7)}$ > NDWI$_{(2-8/2+8)}$ > PCA > NDWI$_{(17/1+7)}$ > MF > OSP > CEM > MF/SAM > MT-TCIMF > SAM. This order suggests that the methods can be grouped by approach and ranked based on their ability to extract snow-covered lakes, is as follows: target detection approach > customized NDWI approach > spectral processing approach (Figure 3b).

The RMSE for the customized NDWI approach varied from ~230 m² to ~314 m². On the other hand, the RMSE of the target detection approach and the spectral processing approach varied from ~97 to 347 m² and from ~307 to ~366 m², respectively. The customized NDWI approach again produced the smallest variation in RMSEs, which reflects that this approach was more stable and consistent for extracting partially snow-covered lakes than the other two approaches.

Comparative Assessment of PAN-Sharpening Algorithms

In this study, we tested five PAN-sharpening algorithms (GS, Wavelet-PC, PC, EF, and BT) for fusing an MS image with PAN. An assessment of the performance of each PAN-sharpening

TABLE 6. QUANTITATIVE EVALUATION (RMSE, M²) OF THE THREE EXTRACTION METHODS PERTAINING TO THE 11 PARTIALLY SNOW-COVERED LAKES USING THE GS-SHARPENED IMAGE

Approach	Method	RMSE (m²)
Target Detection	MT-TCIMF	347.82
	MTMF	273.84
	ACE	97.91
	TCIMF	178.49
	CEM	325.2
	Average	244.65
Customized NDWI	NDWI$_{(1-8/1+8)}$	230.66
	NDWI$_{(2-7/2+7)}$	280.2
	NDWI$_{(1-7/1+7)}$	314.27
	NDWI$_{(2-8/2+8)}$	302.82
	Average	281.99
Spectral Processing	PCA	307.56
	OSP	318.16
	MF/SAM	328.75
	MF	315.47
	SAM	366.99
	Average	327.39

algorithm for lake extraction was undertaken, because the performance of these algorithms is spectrally and/or spatially dependent. From Table 5 (average RMSE), the performance hierarchy of PAN-sharpening algorithms for 14 lake extraction methods, based on RMSE, was GS > Wavelet-PC > PC > EF > BT, which suggests that the GS algorithm outperformed the others, given its small average RMSE (Figure 7).

Wavelet-PC-sharpened and GS-sharpened images performed the best for the TCIMF method (RMSE = 165.001m²) and the NDWI$_{(2-7/2+7)}$ method (RMSE =173.540 m²), respectively (Table 5). PC- and BT-sharpened images performed best for the MTMF method by rendering RMSE of 181.459 and 203.606 m², respectively, while EF showed the best performance for CEM, given its RMSE of 170.814 m². In general, Wavelet-PC and EF are the optimal sharpening algorithms for the target detection approach, while PC and GS are the optimal sharpening algorithms for the customized NDWI approach. BT performed well for the spectral processing approach. Based on the overall RMSE values, the Wavelet-PC-sharpened image coupled with TCIMF (RMSE =165.001 m²) rendered accurate feature extraction, followed closely by the EF-sharpened image coupled with CEM (RMSE =170.814 m²) and the GS-sharpened image coupled with NDWI$_{(2-7/2+7)}$ (RMSE = 173.540 m²). In general, this analysis suggests that GS is the most suitable PAN-sharpening algorithm the greatest number of extraction methods (six methods) followed by Wavelet-PC (three methods) and BT and PC (two methods each). Hence, we concluded that GS-sharpened images provide a decisive tool for semiautomatic extraction of lake features.

Misclassification Statistics for GS-Sharpened Image

In the final step, we tested the performance of all the 14 standalone extraction methods grouped into three semiautomatic lake extraction approaches on the basis of amount of misclassification caused by each method in terms of misclassified number of pixels and equivalent misclassified lake area.

The amount of misclassified areas (percent) for all the 36 lakes and for 11 partially ice or snow covered lake features are summarized in Figure 8. The overall trend of accuracy for the lake extraction methods for all the 36 lakes based on misclassified area (Figure 8) is as follows: NDWI$_{(2-8/2+8)}$ > NDWI$_{(1-7/1+7)}$ > MF > TCIMF > MT-TCIMF > NDWI$_{(2-7/2+7)}$ > (MTMF≈ACE) > OSP > CEM > NDWI$_{(1-8/1+8)}$ > PCA > SAM > MF/SAM. This order suggests that the methods can be grouped by approach and ranked
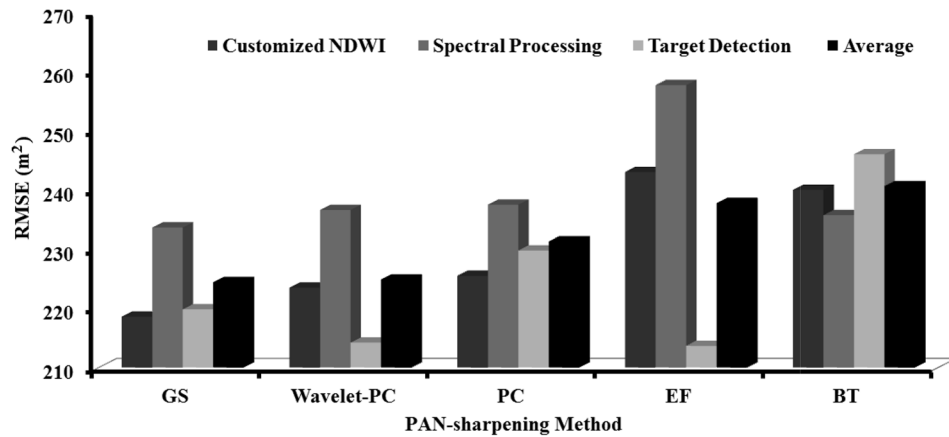
Figure 7. Performance of PAN-sharpening algorithms to produce images that subsequently underwent extraction of lake features using the three semiautomated approaches. The variation of RMSE among the three semiautomatic lake feature extraction approaches is graphically summarized.
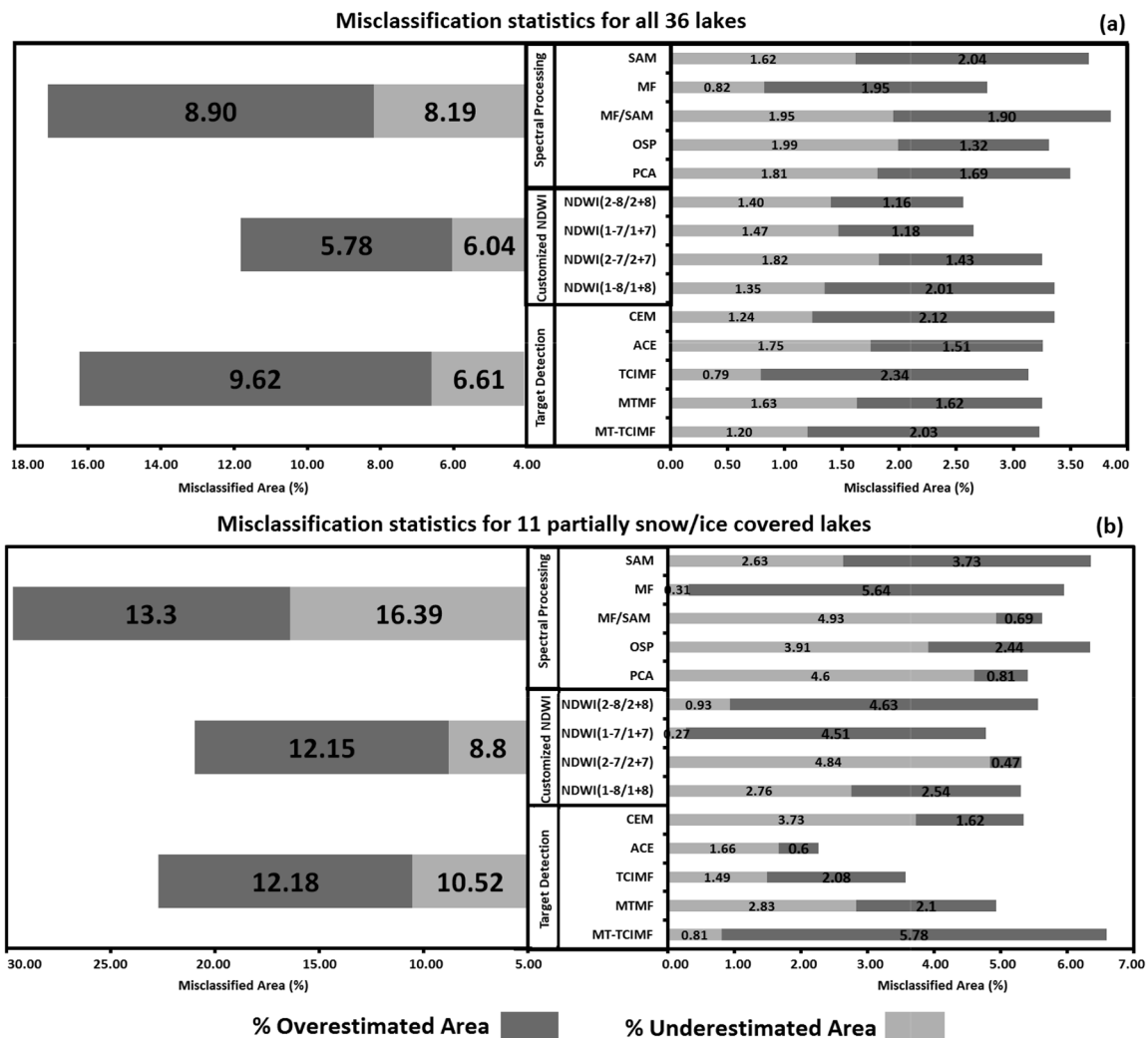

Figure 8. The overall performance of the extraction methods for extracting all the 36 lakes and partially ice/snow-covered 11 lakes, based on misclassified area (percent).

on their ability to extract lakes as follows: customized NDWI approach > target detection approach > spectral processing approach. In general, the customized NDWI rendered a least misclassification (≈12 percent), followed by target detection (≈16 percent) and spectral processing (≈17 percent) methods.

We also found that customized NDWI caused consistently least misclassification (≈21 percent) than the target detection (≈23 percent) and spectral processing (≈30 percent) methods for extraction of partially snow or ice covered 11 lakes (Figure 8).

In order to test the robustness of our analysis and the

validity of customized NDWI approach for extraction of different sizes of lake features, we differentiated the 36 lakes (Table 2) into three groups based on their sizes; small (area < 1,000 m²), medium (1,000 m² < area > 5,000 m²), and large (area > 5,000 m²). From Table 2, it is evident that there are 11 small, 15 medium, and 10 large sized lakes.

The overall trend of accuracy for the lake extraction approaches for 11 small sized lakes based on misclassified area can be expressed as follows: customized NDWI approach (≈48 percent) > spectral processing approach (≈55 percent) > target detection approach (≈56 percent). Similar trend of accuracy for 15 medium sized lakes has been observed as follows: customized NDWI approach (≈13 percent) > spectral processing approach (≈20 percent) > target detection approach (≈22 percent). However, in case of ten large sized lakes, target detection approach performed better than the spectral processing approach. The overall trend for large sized lakes is as follows: customized NDWI approach (≈9 percent) > target detection approach (≈13 percent) > spectral processing approach (≈14 percent). Generally, these trends also suggested that the overall accuracy of lake feature extraction was dependent on the size of the lakes. Broadly, for all the semiautomatic feature extraction approaches, larger errors were observed for small sized lakes (≈48 percent to ≈56 percent), followed by medium sized lakes (≈14 percent to ≈22 percent) and large sized lakes (≈9 percent to ≈14 percent).

Discussion

SIR-based differentiation of land and rock from snow may be relatively straightforward, but the identification of lakes with the landscape is much more problematic. Lakes with the landscape are influenced by the local topography of the study region which confounds the spectral signatures. The Larsemann hills region represents different land covers (snow, ice, rocks, lakes, permafrost, etc.) and with a flat, hilly and mountainous terrain. The characteristic physiographic features of the study region are small, rounded hillocks and broad 'U' shaped glacial valleys exhibiting a rolling topography. The spectral signatures of these lakes are generally confounded because of the surrounding features such as lake water, sediments, and surrounding snow/ice/land surfaces. It is relatively straightforward to extract lake features from flat terrain with low or moderate topographic variations as compared to a hilly terrain, because of the confounding spectral signatures from the surrounding landscape.

A semiautomatic lake feature extraction can be applied in a real operational environment only if it provides superior performance in terms of quality measures. In addition to empirical superiority in terms of accuracy, our analysis shows that the customized NDWI proved to be superior and provides the following advantages over existing extraction methods.

1. Consistency: Customized NDWI based lake feature extraction was less sensitive to the background noise (topography, shadows, and snow/ice cover). Our customized NDWI approach could consistently extract 36 lake features by optimizing the target (water) against the noise.
2. Flexibility: The threshold values used for customized NDWI can be adjusted to suppress the noise without much affecting the extraction of target lakes.
3. Minimization of manual editing: A visual interpretation of extracted lakes showed that the dimension of lake features (shape, geometry, and size) was well preserved and manual editing was highly minimized.
4. Efficiency: The observed average time for extracting lakes was least for customized NDWI, moderate for spectral processing, and maximum for target detection approaches.
5. Interactivity: Our customized NDWI approach is very interactive in terms of threshold definition, and band

selection to rectify the wrongly classified pixels.
6. Robustness:. The customized NDWI method could identify all kinds of lakes in a typical Antarctic coastal oasis environment.
7. Complexity: Customized NDWI approach is easy to implement and less complex, as compared to the target detection or spectral processing algorithms.

In our analysis, the coastal spectral band was normalized against the NIR1 and NIR2 bands. Since the difference in reflectance of each of these spectral bands was greater, it created a discrete threshold for distinguishing regions of standing water. Customized NDWI produces a grayscale image, where water appears bright. Some other features may also appear bright, such as buildings and clouds. However, the likelihood of buildings with spectral response analogous to that of water in the study area is remote. Since the satellite image was captured under minimum cloud cover conditions, water is the only feature that appears bright on the customized NDWI image. The obvious detection of lake features validates the theory that the coastal band is a unique variable in the customized NDWI equation. In the second experiment, the same process was repeated using blue band instead of coastal band. In both the experiments, each customized NDWI ratio produced pragmatic results with lake features of noticeable similarity as evident in both the true/false color composites of the original satellite data and reference digitized data.

Most misclassifications associated with semiautomatic extraction procedures are attributed to four main types of errors:

1. Inaccuracies as a result of cast shadows: If no cast shadow is modeled for a pixel that is actually in a cast shadow, it is highly probable that the pixel will be misclassified as a lake feature. The rate of recurrence and magnitude of these inaccuracies are closely related to the local geography or topography of the study area.
2. Saturation of blue spectral band: Snow and ice exhibits high reflectivity in the visible portion of the electromagnetic spectrum. Pixels with a certain slope and aspect can reflect the incoming sunlight directly into the sensor and cause a saturation of the blue band. This can lead to misclassifications in the customized NDWI approach because of high blue band values.
3. Melt water: The occurrence of melt water on ice and rock surfaces in the austral summer months are not actually misclassifications in technical terms, but can be adjusted for specific extraction of lake features by adjusting threshold values.
4. PAN-sharpening: The process of PAN-sharpening causes spectral and/or spatial distortion in resulting fused images. We attribute the varying amount of spectral and/or spatial distortions in fused images to the five different PAN-sharpening algorithms used in this study.

The prevalent misclassification of cast shadow regions is the main problem with NDWI-based water classification, because the blue band is susceptible to atmospheric scattering. Thus, even in cast shadow regions, there is always a signal in the blue channel. To reduce the shortwave scattering component, DOS was applied to the blue channel, which only produced minor improvements. Hence, for extraction of water cover, it is necessary to check the lake areas covered by cast shadow, or these areas may be underestimated or overestimated as a result of false negative or positive signals. However, in this study, there were only a few of these errors, as shown in the final stage of extraction. To avoid an unacceptable number of misclassifications The accuracy assessment of the digitized vector data was necessary as it is the most crucial reference data used in this study. A perpendicular error distance from the digitized shoreline vertex to the DGPS reference shoreline

vertex was calculated for ten random points per lake, i.e., 360 points for 36 lake features. The perpendicular distance errors were found to vary from ≈3 mm to ≈11 mm (RMSE ≈9 mm). Additionally, to check the effect of digitization errors on overall lake area, each digitized lake polygon area value was compared with the original reference DGPS based lake area value. The difference in lake area values varied from ≈4 m² to ≈7 m² with RMSE of ≈5.7 m². The quantitative error in digitization (positional error RMSE of ≈9 mm and RMSE in lake area of ≈5.7 m²) is insignificant as compared to the errors caused by different extraction methods (≈220 m² to ≈260 m²), for extraction of 36 lake features. Moreover, the digitization error amount would be constant for all 14 lake extraction methods, and hence, the comparison of these methods in present analysis would be unbiased and valid.

Conclusions

The spectral characteristics of cryospheric lakes from WV-2 images were analyzed by utilizing a combination of image processing methods. The use of well-established PAN-sharpening algorithms coupled with a numerous number of feature extraction methods provided an effective platform to support semiautomatic extraction of Antarctic lake features. The use of all NDWI combinations derived by using the duplet set of VNIR bands offered a wide and precise means for extracting lake areas. The degree and extent (magnitude) of the spectral and/or spatial distortions introduced by PAN-sharpening influenced consequent extraction processing, and significantly influenced the final accuracy of the analysis. Incorporating the unique add-on WV-2 bands offered a contextual foundation for surface mapping by using feature extraction methods and scene characterization, in contrast to other commercial MS image sensors. Different band combinations of NDWI provide a broad vision to resolve minor variations in the performance of the practiced extraction procedures, which would have not been possible with other satellite data that contained only the single infrared, red, and blue bands. The different band combinations used in this study also facilitated a deep understanding of the role of specific spectral bands used in diverse combinations in order to produce the best extraction from PAN-sharpened images. This work suggests that data from the add-on WV-2 bands which allow for a unique set of NDWIs can be coupled with traditional PAN-sharpening algorithms to create superior methods for feature extraction.

Acknowledgments

References

Boardman, J.W., 1998. Leveraging the high dimensionality of AVIRIS data for improved sub-pixel target unmixing and rejection of false positives: Mixture tuned matched filtering, *Proceedings of the Seventh JPL Airborne Earth Science Workshop, AVIRIS*, JPL Publication 97-21.

Bourennane, S., C. Fossati, and A. Cailly, 2011. Improvement of target-detection algorithms based on adaptive three-dimensional filtering, *IEEE Transactions on Geoscience and Remote* Sensing, 49(4):1383–1395.

Box, J.E., and K. Ski, 2007. Remote sounding of Greenland supraglacial melt lakes: Implications for subglacial hydraulics, *Journal of Glaciology*, 53(181):257–265.

Chang, C-I, J.M. Liu, B.C. Chieu, C.M. Wang, C.S. Lo, P.C. Chung, H. Ren, C.W. Yang, and D.J. Ma, 2000. Generalized constrained energy minimization approach to sub-pixel target detection for multispectral imagery, *Optical Engineering*, 39(5):1275–1281.

Chavez, P.S., 1996. Image-based atmospheric corrections-revisited and improved, *Photogrammetric Engineering & Remote Sensing,* 62(9):1025–1036.

Chavez, P.S., S.C. Sides, and J.A. Anderson, 1991. Comparison of three different methods to merge multiresolution and multispectral data: Landsat TM and SPOT panchromatic, *Photogrammetric Engineering & Remote Sensing*, 57(3):295–303.

Congalton, R., 2008. Thematic and positional accuracy assessment of digital remotely sensed data, *Proceedings of the 7th Annual Forest Inventory and Analysis Symposium* (R. Roberts, G. Reams, P. Van Deusen, and P. McWilliams, editors) General Technical Report WO-77, USDA Forest Service, pp. 149–154.

Congalton, R.G., 1991. A review of assessing the accuracy of classifications of remotely sensed data, *Remote Sensing of Environment*, 37:35–46.

Congalton, R.G., and K. Green, 1999. *Assessing the Accuracy of Remotely Sensed Data: Principles and Practices*, Lewis Publishers, Boca Raton, Florida.

Frazier, P.S., and K.J. Page, 2000. Water body detection and delineation with Landsat TM data, *Photogrammetric Engineering & Remote Sensing*, 6(12):1461–1467.

Hallada, W.A., and S. Cox, 1983. Image sharpening for mixed spatial and spectral resolution satellite systems, *Proceedings of the 17th International Symposium on Remote Sensing of the Environment*, 09-13 May, Ann Arbor, Michigan, pp. 1023–1032.

Harris, U., 2008. Larsemann Hills - Mapping from aerial photography captured February 1998. *Australian Antarctic Data Centre - CAASM Metadata*: URL: *http://data.aad.gov.au/aadc/metadata/* (last date accessed: 28 July 2014).

Harsanyi, J.C., and C.-I. Chang, 1994. Hyperspectral image classification and dimensionality reduction: An orthogonal subspace projection approach, *IEEE Transactions on Geoscience and Remote Sensing*, 32(4):779–785.

Hu, X., Z. Zhang, and C.V. Tao, 2004. A robust method for semi-automatic extraction of road centerlines using a piecewise parabolic model and least square template matching, *Photogrammetric Engineering & Remote Sensing*, 70(12):1393–1398.

Huggel, C., A. Kaab, W. Haeberli, P. Teysseire, and F. Paul, 2002. Remote sensing based assessment of hazards from glacier lake outbursts: A case study in the Swiss Alps, *Canadian Geotechnical Journal*, 39:316–330.

Jawak, S.D., and A.J. Luis, 2013a. A spectral index ratio-based Antarctic land-cover mapping using hyperspatial 8-band WorldView-2 imagery, *Polar Science*, 7(1):18–38, URL: *http://dx.doi.org/10.1016/j.polar.2012.12.002* (last date accessed: 28 July 2014)

Jawak, S.D., and A.J. Luis, 2013b. Improved land cover mapping using high resolution multiangle 8-band WorldView-2 satellite remote sensing data, *Journal of Applied Remote Sensing*, 7(1):073573, doi:10.1117/1.JRS.7.073573.

Jia, X., and J.A. Richards, 1999. Segmented principal components transformation for efficient hyperspectral remote-sensing image display and classification, *IEEE Transactions on Geoscience and Remote Sensing*, 37(1, Part 2):538–542.

Jin, X., S. Paswaters, and H. Cline, 2009. A comparative study of target detection algorithms for hyperspectral imagery, *Algorithms*

and Technologies for Multispectral, Hyperspectral, and Ultraspectral Imagery, *Proceedings of SPIE 7334*, 13 April, Orlando, Florida, 73341W1-73341W12, doi:10.1117/12.818790.

Johansson A.M., and I.A. Brown, 2013. Adaptive Classification of Supra-Glacial Lakes on the West Greenland Ice Sheet, *IEEE Journal of Selected Topics in Applied Earth Observations and Remote Sensing*, 6(4):1998–2007.

Klonus, S., and M. Ehlers, 2007. Image fusion using the Ehlers spectral characteristics preserving algorithm, *GIScience & Remote Sensing*, 44(2):93–116.

Kruse, F.A., A.B. Lefkoff, J.W. Boardman, K.B. Heidebrecht, A.T. Shapiro, J.P. Barloon, and A.F. Goetz, 1993. The spectral image processing system (SIPS) - Interactive visualization and analysis of imaging spectrometer data, *Remote Sensing of Environment*, 44:145–163.

Laben, C.A., V. Bernard, and W. Brower, 2000. *Process for Enhancing The Spatial Resolution of Multispectral Imagery Using Pan-Sharpening*, US Patent No. 6, 011,875, Eastman Kodak Company, Technical Report.

Lacaux, J.P., Y.M. Tourre, C. Vignolles, J.A. Ndione, and M. Lafaye, 2007. Classification of ponds from high-spatial resolution remote sensing: Application to Rift Valley Fever epidemics in Senegal, *Remote Sensing of Environment*, 106(1):66–74.

Lampkin, D.J., and J. VanderBerg, 2011. A preliminary investigation of the influence of basal and surface topography on supraglacial lake distribution near Jakobshavn Isbræ, western Greenland, *Hydrological Processes*, 25 (21):3347–3355.

Li, B., and X.Z. Zhou, 2009. Research on extraction method of river water-body in mountain area of western Sichuan based on MODIS data, *Geography and Geo-Information Science*, 25:59–62.

Lu, S., B. Wu, N. Yan, and, H. Wang, 2011. Water body mapping method with HJ-1A/B satellite imagery, *International Journal of Applied Earth Observation and Geoinformation*, 13(3):428–434, URL: *http://dx.doi.org/10.1016/j.jag.2010.09.006* (last date accessed: 28 July 2014)

Lüthje, M., L.T. Pederson, N. Reeh, and W. Greuell, 2006. Modelling the evolution of supraglacial lakes on the West Greenland Ice-Sheet margin, *Journal of* Glaciology, 52(179):608–618, URL: *http://dx.doi.org/10.3189/172756506781828386* (last date accessed: 28 July 2014).

McFeeters, S.K., 1996. The use of the Normalized Difference Water Index (NDWI) in the delineation of open water features, *International Journal of Remote Sensing*, 17:1425– 1432.

McFeeters, S.K., 2013. Using the Normalized Difference Water Index (NDWI) within a Geographic Information System to detect swimming pools for mosquito abatement: A practical approach, *Remote Sensing*, 5:3544–3561.

McMillan, M., P. Nienow, A. Shepherd, T. Benham, and A. Sole, 2007. Seasonal evolution of supra-glacial lakes on the Greenland Ice Sheet, *Earth and Planetary Science Letters*, 262:484–492, URL: http://dx.doi.org/10.1016/j.epsl.2007.08.002 (last date accessed: 28 July 2014).

Ouma, Y.O., and R. Tateishi, 2006. A water index for rapid mapping of shoreline changes of five East African Rift Valley lakes: An empirical analysis using Landsat TM and ETM+ data, *International Journal of Remote Sensing*, 27:3153–3181.

Peng, H., F. Long, and C. Ding, 2005. Feature selection based on mutual information: Criteria of max-dependency, max-relevance and min-redundancy, *IEEE Transactions of Pattern Analysis and Machine Intelligence*, 27(8):1667–1238, URL: *http://dx.doi.org/10.1109/TPAMI.2005.159* (last date accessed: 28 July 2014).

Peterson, M.R., T. Horner, and F. Moore, 2011. Evolving matched filter transform pairs for satellite image processing, *Proceedings of SPIE 8059, Evolutionary and Bio-Inspired Computation: Theory and Applications (80590L)*, 25 April, Orlando, Florida, doi:10.1117/12.884312.

Pradhan, P., R. King, N.H. Younan, and D.W. Holcomb, 2006. The effect of decomposition levels in wavelet-based fusion for multiresolution and multi-sensor images, *IEEE Transactions on Geoscience and Remote Sensing*, 44(12):3674–3686.

Ren, H., and C.-I. Chang, 2000. Target-constrained interference-minimized approach to subpixel target detection for hyperspectral imagery, *Optical Engineering*, 39(12):3138–3145.

Rogers, A.S., and M.S. Kearney, 2004. Reducing signature variability in unmixing coastal marsh Thematic Mapper scenes using spectral indices *International Journal of Remote Sensing*, 20: 2317–2335.

Selmes, N., T. Murray, and T.D. James, 2011. Fast draining lakes on the Greenland Ice Sheet, *Geophysical Research Letters*, 38, L15501.

Sneed, W.A., and G.S. Hamilton, 2007. Evolution of melt pond volume on the surface of the Greenland ice sheet, *Geophysical Research Letters*, 34, L03501, doi:10.1029/2006GL028697.

Soti, V., A. Tran, J. Bailly, C. Puech, and D.L. Seen, and A. Bégué, 2009. Assessing optical earth observation systems for mapping and monitoring temporary ponds in arid areas, *International Journal of Applied Earth Observation and Geoinformation*, 11:344–351.

Sundal, A.V., A. Shepherd, P. Nienow, E. Hanna, S. Palmer, and P. Huybrechts, 2009. Evolution of supra-glacial lakes across the Greenland Ice Sheet, *Remote Sensing of Environment*, 113:2164–2171, URL: *http://dx.doi.org/10.1016/j.rse.2009.05.018* (last date accessed: 28 July 2014).

Tedesco, M., and N. Steiner, 2011. In-situ multispectral and bathymetric measurements over a supraglacial lake in western Greenland using a remotely controlled watercraft, *The Cryosphere,* 5 (2):445–452, doi:10.5194/tcd-5-479-2011.

Updike T., and C. Comp, 2010. *Radiometric Use of WorldView-2 Imagery, Technical Note*, DigitalGlobe®, Colorado, URL: *http://www.digitalglobe.com/sites/default/files/Radiometric_Use_of_WorldView-2_Imagery%20%281%29.pdf* (last date accessed: 28 July 2014)

Wessels, R., J. Kargel, and H. Kieffer, 2002. ASTER measurement of supraglacial lakes in the Mount Everest region of the Himalaya, *Annals of Glaciology,* 34:399–408.

Williams, A.P., and E.R. Hunt, 2002. Estimation of leafy spurge cover from hyperspectral imagery using mixture tuned matched filtering, *Remote Sensing of Environment*, 82(2- 3):446–456.

Wu, W.Y., X.H. Shen, L.J. Zou, S.L. Lu, and G.F. Zhang, 2008. An integrated method for water body detection and delineation using Landsat ETM+ data, *Bulletin of Science and Technology*, 24:252–259.

Xiao, X.M., S. Boles, J.Y. Liu, D. F. Zuang, S. Frolking, C.S. Li, W. Salas, and B. Moore III, 2005. Mapping paddy rice agriculture in southern China using multi-temporal MODIS images, *Remote Sensing of Environment,* 95:480–492.

Xie, Z., D. ShangGuan, S. Zhang, Y. Ding, S. Liu, 2013. Index for hazard of Glacier Lake outburst flood of Lake Merzbacher by satellite-based monitoring of lake area and ice cover, *Global and Planetary Change*, 107:229–237.

Xu, H., 2005. A study on information extraction of water body with the modified normalized difference water index (MNDWI), *Journal of Remote Sensing*, 9(005):589–595.

Zhang, Y., 2002. Problems in the fusion of commercial high resolution satellite images as well as Landsat 7 images and initial solutions, *ISPRS, CIG, SDH Joint International Symposium on GeoSpatial Theory, Processing and Applications*, Ottawa, Canada, 08-12 July, *International Archives of Photogrammetry and Remote Sensing*, Volume 34, Part 4)

Zhong, C. Q., C.S. Zeng, and Z.Z. Liu, 2008. Study on terrestrial water information identified based on the analysis of spectral signature and ratio index, *Geography and Geo- Information Science*, 10:663–669.